

Shear-driven and pressure-driven flow of a nematic liquid crystal in a slowly varying channel

J. Quintans Carou, B. R. Duffy, N. J. Mottram and S. K. Wilson*

*Department of Mathematics, University of Strathclyde, Livingstone Tower,
26 Richmond Street, Glasgow G1 1XH, United Kingdom*

Abstract

Motivated by the industrially important processes of blade coating and cavity filling of liquid crystalline materials, we consider steady, two-dimensional shear-driven (Couette) and pressure-driven (plane Poiseuille) flow of a thin film of a nematic liquid crystal in the slowly varying channel formed between a fixed blade of prescribed shape and a planar substrate. Specifically, blade coating motivates the study of shear-driven flow due to the motion of the substrate parallel to itself with constant velocity, while cavity filling motivates the study of pressure-driven flow due to an imposed pressure drop. We use a combination of analytical and numerical techniques to analyse the Ericksen–Leslie equations governing the fluid velocity and pressure and the director orientation in cases when both the aspect ratio of the channel and the distortion of the director field are small. We demonstrate a variety of flow and director-orientation patterns occurring in different parameter regimes. In the limit of weak flow effects flow alignment does not occur and the appropriate solution of the governing equations is found explicitly. In the limit of strong flow effects flow alignment occurs and orientational boundary layers exist near the substrate and near the blade, and, in addition, an orientational internal layer may also exist within which the director orientation changes from $+\theta_0$ to $-\theta_0$, where θ_0 is the flow-alignment angle.

* Author to whom correspondence should be addressed. Electronic mail: s.k.wilson@strath.ac.uk

I. INTRODUCTION

A thermotropic liquid crystal is an anisotropic liquid consisting of rod-like (calamitic) or disc-like (discotic) molecules that exists as an intermediate state between a crystalline solid and an isotropic liquid. The major commercial interest in liquid crystals is a consequence of their optical properties which are exploited in display technologies. These optical properties are directly related to the mean orientation of the molecules in the liquid crystal which can be described by a macroscopic variable, a unit vector called the director. In recent years liquid crystal coating and filling processes have been investigated in order to facilitate more efficient mass production of liquid crystal displays.¹ A crucial element of a commercially successful mass production process is the reliable manufacture of homogeneous and defect-free layers of liquid crystal. Blade-coating processes typically use a blade on one side of which there is a reservoir of liquid crystal, and under which the substrate to be coated is pulled. The liquid crystal is then coated onto the substrate in a thin film, as shown in Fig. 1. Cavity-filling processes typically impose a pressure drop in order to drive the liquid crystal into a gap between fixed boundaries.

The aim of the present work is to advance the understanding of the behaviour of a nematic liquid crystal during coating and filling processes. Although, at present, in an industrial setting, these processes are usually undertaken while the material is in the isotropic phase, we will investigate the alignment behaviour in the nematic phase. This will give insight into how flow effects may influence alignment within the coated layer or the filled channel. In particular, flow effects during coating or filling in the nematic phase may lead to enhanced director alignment and hence a reduction in the possibility of defects occurring in the final product, which would be of great interest to device manufacturers. We tackle the problem using the Ericksen–Leslie equations^{2–5} for

a nematic liquid crystal. These equations have consistently been successfully applied to many liquid crystal switching and flow problems,⁵ and we can have confidence that they will accurately model the present system.

Pikin⁶ studied a one-dimensional model of the influence of shear on the orientation of a nematic liquid crystal and obtained some approximate solutions of the Ericksen–Leslie equations. He proved the existence and stability of different types of director behaviour depending on the material parameters. In particular, for strong shear he predicted the existence and thickness of thin orientational boundary layers in which the director orientation changes rapidly from its boundary-dictated value to the flow-alignment angle θ_0 (the alignment of the director to the streamlines induced by shear in the absence of other effects³) in the bulk. MacSithigh and Currie⁷ also studied approximate solutions for the director orientation for strong shear, and in a subsequent paper Currie and MacSithigh⁸ studied the stability and dissipation of these solutions. Similar solutions were also investigated by Skarp and Carlsson⁹ who considered the influence of an electric field on the director orientation for strong shear both theoretically and experimentally. Pressure-driven flow was considered by Atkin,¹⁰ who studied the existence and uniqueness of an exact solution of the Ericksen–Leslie equations for steady flow in an infinitely long circular cylinder or between two coaxial cylinders. Later, Currie¹¹ discussed the same problem and found approximate solutions for the director. Rey and Denn¹² obtained a similarity solution of the Ericksen–Leslie equations for flow of prescribed flux between converging and diverging planar boundaries (Jeffery–Hamel flow).

Many issues in nematic liquid crystal flows have been investigated by solving the Ericksen–Leslie equations numerically. For instance, Derfel¹³ considered in-plane alignment of the director during simple shear flow, and subsequently Derfel and Radomska¹⁴ considered out-of-plane alignment; more recently, Tu *et al.*¹⁵ considered different ap-

proximations of the liquid crystal elastic constants to analyse the effect of the elastic anisotropy on the director orientation. More complex geometries have been considered in studies of pressure-driven flows; for instance, Rey¹⁶ studied radial flow between concentric parallel discs and showed the existence of orientational boundary layers, Chono and Tsuji¹⁷ analysed flow around a circular cylinder, and Chang *et al.*¹⁸ developed a new numerical method to study the flow of liquid crystals in complex geometries. Other numerical studies considered transient flows in order to describe the behaviour of nematic liquid crystals subject to director tumbling^{19,20} or to study the effect of the elastic anisotropy on the flow and the director.²¹

Some analytical work on oscillatory flows has been carried out by Krekhov *et al.*²² and more recently by de Andrade Lima and Rey²³ who described a method to distinguish between flow-aligning and non-flow-aligning nematic liquid crystals.

Although the Ericksen–Leslie theory has been successful in modelling many nematic liquid crystal flows, other theories are also widely used. For instance, Ericksen²⁴ developed a theory that includes the order parameter of the liquid crystal, and this theory has been considered by Calderer and Liu²⁵ in a study of pressure-driven flows. Other theories commonly considered include the Doi theory, which was used by, for instance, Feng and Leal²⁶ to describe how the geometry of the channel influences the orientation of the liquid crystal during pressure-driven flow, and a more general theory due to Tsuji and Rey that incorporates both Ericksen–Leslie and Doi theories as special cases, which was considered by, for instance, Rey and Tsuji.²⁷ These theories are outside the scope of this paper and the reader is referred to the review by Rey and Denn²⁸ for more details.

In this paper we address steady, two-dimensional shear-driven (Couette) and pressure-driven (plane Poiseuille) flow of a thin film of a nematic liquid crystal in the slowly varying channel formed between a fixed blade of prescribed shape and a planar substrate,

as shown in Fig. 2. We adopt a new approach to the problems involving a combination of analytical and numerical techniques to analyse the Ericksen–Leslie equations^{2–5} governing the fluid velocity and pressure and the director orientation. In contrast to the previous analytical results discussed above we are able to give analytical or semi-analytical solutions for both shear-driven and pressure-driven flow without using, for example, a “one-constant” approximation to the elastic constants, and without restricting the analysis to one spatial dimension. Some of the present results for shear-driven flow (in particular, some of those in Sec. III C) were recently presented at an international liquid crystal conference.²⁹

We demonstrate a variety of flow and director-orientation patterns occurring depending on the system and material parameters. Using justifiable assumptions to identify situations in which there is a decoupling between flow and director enables us to give explicit closed-form solutions for the velocity and the director in three of the five cases described. Of crucial importance is the *Ericksen number*, a non-dimensional parameter measuring the relative strength of viscosity and orientational elasticity effects.

We find that in the limit of weak flow effects (i.e. small Ericksen number) flow alignment does not occur and, in such cases, the director orientation is influenced predominantly by the boundary conditions. Critical values of the Ericksen number for which there is a qualitative change in the director profile are given explicitly; this characterisation of the director during the coating or cell-filling process is of importance since it may indicate when defects are likely to occur in the final product.

In the limit of strong flow effects (i.e. large Ericksen number), flow alignment occurs and orientational boundary layers exist near the substrate and near the blade, and, in addition, an orientational internal layer may also exist within which the director orientation changes from $+\theta_0$ to $-\theta_0$. Such a change in the orientation from $+\theta_0$ to $-\theta_0$

would be undesirable since it could conceivably lead to defects in the final display. We present a parameter plane showing when orientational internal layers occur.

As a final remark, we emphasise that the present analysis is valid for *any* blade shape, and so our model can be used to describe a great number of coating or cell-filling processes.

II. GOVERNING EQUATIONS

Consider steady, two-dimensional flow of a thin film of a nematic liquid crystal between a fixed blade of prescribed shape and a planar substrate. The substrate is taken to lie in the plane $z = 0$ whilst the blade is taken to lie at $z = h(x)$, a prescribed function of x , the coordinate in the direction of the imposed shear or pressure drop, as shown in Fig. 2. The substrate is moved to the right at a constant speed U (> 0) (shear-driven flow) or a pressure drop $p_0 - p_L$ (> 0) is imposed across the liquid crystal underneath the blade in the x direction between $x = 0$ and $x = L$ (pressure-driven flow). We assume that all dependent variables are functions of x and z only. The nematic director \mathbf{n} is assumed to lie within the plane of shear, which is a justifiable assumption for realistic values of the shear, and the fluid velocity \mathbf{v} is assumed to have components only in the x and z directions, which is also a justifiable assumption if \mathbf{n} remains in the x - z plane. The director, fluid velocity and pressure may therefore be written as

$$\mathbf{n} = (\cos \theta(x, z), 0, \sin \theta(x, z)) \quad (1)$$

$$\mathbf{v} = (u(x, z), 0, w(x, z)), \quad (2)$$

$$p = p(x, z), \quad (3)$$

where the director angle $\theta = \theta(x, z)$ is the angle that the director makes with the positive x axis.

The Ericksen–Leslie dynamical equations^{2–5} consist of a mass-conservation equation and balance laws of linear and angular momentum; in the present situation and with inertia and external forces neglected the equations simplify to

$$v_{i,i} = 0, \quad (4)$$

$$0 = -\tilde{p}_{,i} + \tilde{g}_k \frac{\partial n_k}{\partial \theta} \theta_{,i} + \tilde{t}_{ik,k}, \quad (5)$$

$$\left(\frac{\partial W}{\partial \theta_{,i}} \right)_{,i} - \frac{\partial W}{\partial \theta} + \tilde{g}_i \frac{\partial n_i}{\partial \theta} = 0. \quad (6)$$

The standard redefinition of pressure used when studying the Ericksen–Leslie equations has been employed so that the modified pressure \tilde{p} includes a term dependent on orientational elasticity, i.e. $\tilde{p} = p + W$, where W is the elastic energy. The constitutive laws for $\tilde{\mathbf{g}}$, $\tilde{\mathbf{t}}$ and W are

$$\tilde{g}_i = -\gamma_1 N_i - \gamma_2 A_{ij} n_j, \quad (7)$$

$$\tilde{t}_{ij} = \alpha_1 (n_k n_p A_{kp}) n_i n_j + \alpha_2 N_i n_j + \alpha_3 N_j n_i + \alpha_4 A_{ij} + \alpha_5 A_{ik} n_k n_j + \alpha_6 A_{jk} n_k n_i, \quad (8)$$

$$2W = K_1 (\nabla \cdot \mathbf{n})^2 + K_2 (\mathbf{n} \cdot \nabla \times \mathbf{n})^2 + K_3 [(\mathbf{n} \cdot \nabla) \mathbf{n}]^2, \quad (9)$$

where

$$\gamma_1 = \alpha_3 - \alpha_2, \quad \gamma_2 = \alpha_6 - \alpha_5, \quad (10)$$

with α_i ($i = 1, \dots, 6$) the Leslie viscosities and K_i ($i = 1, 2, 3$) the elastic constants for splay, twist and bend, and the Parodi relation $\alpha_6 - \alpha_5 = \alpha_2 + \alpha_3$ is assumed to hold. The rate-of-strain tensor \mathbf{A} , the co-rotational time derivative of the director \mathbf{N} and the vorticity tensor \mathbf{W} are given respectively by

$$A_{ij} = \frac{1}{2}(v_{i,j} + v_{j,i}), \quad N_i = \dot{n}_i - W_{ij} n_j, \quad W_{ij} = \frac{1}{2}(v_{i,j} - v_{j,i}), \quad (11)$$

where a superposed dot denotes the usual material time derivative $\partial/\partial t + \mathbf{v} \cdot \nabla$.

We use the following non-dimensionalisation of the independent variables and parameters:

$$x = Lx^*, \quad z = Hz^*, \quad h = Hh^*, \quad \alpha_i = \mu_0\alpha_i^*, \quad K_i = K_0K_i^*, \quad (12)$$

where μ_0 is a combination of the Leslie viscosities α_i , K_0 is one of the elastic constants K_i , H is a typical value of h , and L is the length of the blade in the x direction. In the case of shear-driven flow the appropriate non-dimensionalisation of the fluid velocity and pressure is

$$u = Uu^*, \quad w = \frac{HU}{L}w^*, \quad \tilde{p} - p_L = \frac{\mu_0UL}{H^2}\tilde{p}^*, \quad (13)$$

whereas in the case of pressure-driven flow it is

$$u = \frac{H^2(p_0 - p_L)}{\mu_0L}u^*, \quad w = \frac{H^3(p_0 - p_L)}{\mu_0L^2}w^*, \quad \tilde{p} - p_L = (p_0 - p_L)\tilde{p}^*. \quad (14)$$

The length and velocity in the x and z directions have been non-dimensionalised differently to reflect the slenderness of the slowly varying channel formed between the blade and the substrate, and the standard ‘‘lubrication’’ scaling of the pressure has been employed.^{31,32}

When presenting results, we will consider two specific blade shapes, namely $h(x) = 1 - \alpha(1 - x)$ with $\alpha < 0$ and $h(x) = 1 + \alpha x$ with $\alpha > 0$, corresponding to a linearly converging and a linearly diverging channel, respectively. However, the present analysis is valid for *any* blade shape.

In general, very little analytical progress can be made since the governing equations are coupled partial differential equations that involve nonlinear functions of θ . For instance, in the momentum equations the effective viscosity α_{eff} is a nonlinear function of θ :

$$\alpha_{\text{eff}} = \frac{1}{2}(\alpha_4 + \alpha_3 + \alpha_6)\cos^2\theta + \frac{1}{2}(\alpha_4 + \alpha_5 - \alpha_2)\sin^2\theta + \alpha_1\cos^2\theta\sin^2\theta. \quad (15)$$

In order to make analytical progress, we will make some justifiable approximations, as described in the next two sections.

A. Thin-film approximation

The first approximation we make is a thin-film approximation^{31,32} based on the assumption that the aspect ratio ϵ of the channel, defined by $\epsilon = H/L$, is small, that is, $\epsilon \ll 1$. In the limit $\epsilon \rightarrow 0$ the linear momentum and the angular momentum balances in the Ericksen–Leslie equations (5) and (6) (with the superscript star dropped from the non-dimensional variables) are

$$0 = \tilde{p}_x - (g(\theta)u_z)_z + O(\epsilon), \quad (16)$$

$$0 = \tilde{p}_z + O(\epsilon), \quad (17)$$

$$0 = Em(\theta)u_z - \left[f(\theta)\theta_{zz} + \frac{1}{2}f'(\theta)\theta_z^2 \right] + O(\epsilon), \quad (18)$$

where

$$g(\theta) = \eta_1 \cos^2 \theta + \eta_2 \sin^2 \theta + \alpha_1 \cos^2 \theta \sin^2 \theta, \quad (19)$$

$$f(\theta) = K_1 \cos^2 \theta + K_3 \sin^2 \theta, \quad (20)$$

$$m(\theta) = \alpha_3 \cos^2 \theta - \alpha_2 \sin^2 \theta, \quad (21)$$

in which $\eta_1 = (\alpha_4 + \alpha_3 + \alpha_6)/2$ and $\eta_2 = (\alpha_4 + \alpha_5 - \alpha_2)/2$ are two of the so-called Miesowicz viscosities.³³ A derivation of the thin-film equations (16)–(18) is presented in the Appendix. Appropriate choices for μ_0 and K_0 in (12) are $\mu_0 = \eta_1$ and $K_0 = K_1$. The non-dimensional parameter E is the Ericksen number defined by $E = \eta_1 UH/K_1$ and $E = H^3(p_0 - p_L)/K_1 L$ in shear-driven and pressure-driven flow, respectively.

In the case of shear-driven flow the leading order non-dimensional boundary conditions on u , θ and \tilde{p} are

$$u = 1, \quad \theta = 0 \quad \text{on} \quad z = 0, \quad (22)$$

$$u = 0, \quad \theta = \epsilon h_x \quad \text{on} \quad z = h, \quad (23)$$

$$\tilde{p} = 0 \quad \text{at} \quad x = 0, \quad (24)$$

$$\tilde{p} = 0 \quad \text{at} \quad x = 1, \quad (25)$$

while in the case of pressure-driven flow (22) and (24) are replaced by

$$u = 0, \quad \theta = 0 \quad \text{on} \quad z = 0, \quad (26)$$

$$\tilde{p} = 1 \quad \text{at} \quad x = 0. \quad (27)$$

The boundary conditions on u and θ correspond respectively to no slip and strong homogeneous orientation (i.e. the director lies parallel to the boundary) at both boundaries. There will be a three-phase contact line on the blade at the channel exit; the form that the director will take near such a contact line is unclear, and is the subject of much ongoing discussion.^{32,34,35} Behaviour other than that specified by the boundary condition (23) at $x = 1$ and $z = h(1)$ is certainly possible, but for simplicity we retain (23), in the expectation that the predicted solution overall would be qualitatively unaffected if an alternative condition were imposed. The boundary conditions on \tilde{p} follow from (17), which requires that the pressure at either end of the blade is constant, and from the fact that, since the pressure enters the Ericksen–Leslie equations only through derivative terms, and is therefore degenerate up to an additive constant, we can take the rescaled pressure to be equal to zero at $x = 0$ and $x = 1$ in shear-driven flow and equal to unity at $x = 0$ and zero at $x = 1$ in pressure-driven flow.

The nonlinear dependence of $g(\theta)$, $f(\theta)$ and $m(\theta)$ on θ means again that, in general, no significant analytical progress can be made. In order to make any progress we will consider a second approximation concerning the size of θ .

B. Director approximations

The boundary conditions on θ are $\theta = 0$ at $z = 0$ and $\theta = \epsilon h_x$ at $z = h$, and it is therefore possible that θ remains no larger than $O(\epsilon)$ throughout the channel. Since no external torques (such as those induced by an applied electric field) are present, the only internal torque that might cause θ to be larger than $O(\epsilon)$ is that due to the fluid flow. In a flow-aligning material (i.e. one with $\alpha_2\alpha_3 > 0$) the flow effects will tend to align the director so that $\theta = \pm\theta_0$, where $\theta_0 = \tan^{-1} \sqrt{\alpha_3/\alpha_2}$ is the flow-alignment angle, whereas in a non-flow-aligning material (i.e. one with $\alpha_2\alpha_3 < 0$) a flow-alignment angle does not exist, and the flow will cause the director to rotate continuously (“tumble”). For definiteness we assume that $\alpha_2 < 0$ (as it is for calamitic liquid crystals) and $\alpha_3 < 0$, so that the material is flow-aligning, i.e. θ_0 is defined; however, as we shall describe in Sec. V, the present analysis is also relevant to other cases. In flow-aligning materials, α_3 is typically two orders of magnitude smaller than α_2 , and so θ_0 is usually small. Therefore, the maximum director angle in the layer is at least as large as ϵ , since it attains this value at the blade, and, if $\theta_0 > \epsilon$, will be no larger than θ_0 , since this is the maximum value that flow aligning can achieve. Therefore, since both ϵ and θ_0 are small, we can confidently assert that $\theta \ll 1$, i.e. that the distortion of the director field is small.

We now have three small parameters to consider: the aspect ratio ϵ , a director-angle scale δ which is defined by $\theta = \delta\theta^*$, where $\theta^* = O(1)$, and the flow-alignment angle θ_0 . Since, as explained above, θ cannot be smaller than ϵ everywhere in the channel, there are two main cases to consider: $\delta = O(\epsilon)$ and $\delta \gg \epsilon$. Within these two main cases we must consider various subcases depending on the size of the parameter θ_0 . If the flow has only a weak effect on the director then $\delta \ll \theta_0$. If, however, the flow aligns the director then $\delta = O(\theta_0)$. Finally, if the blade aligns the director at an angle much greater than

the flow-alignment angle then $\delta \gg \theta_0$.

Case 1: $\epsilon \sim \delta \ll 1$, i.e. θ is of a similar size to its value at the blade.

In this case there are three subcases to consider.

Case 1a: $\delta \ll \theta_0$: flow effects are insufficient to increase θ significantly from the boundary-dictated value and flow alignment is not achieved.

Case 1b: $\delta \sim \theta_0$: flow effects are sufficiently strong to achieve flow alignment in part of the channel.

Case 1c: $\delta \gg \theta_0$: the flow-alignment angle is much less than the boundary-dictated value of θ ; flow alignment may occur, but θ will attain its maximum value at the blade.

Case 2: $\epsilon \ll \delta \ll 1$, i.e. θ is much larger than its value at the blade.

In this case there are again three subcases to consider.

Case 2a: $\delta \ll \theta_0$: flow effects increase θ significantly above the boundary-dictated value, but they are not sufficiently strong to achieve flow alignment.

Case 2b: $\delta \sim \theta_0$: flow effects are sufficiently strong to achieve flow alignment in part of the channel.

Case 2c: $\delta \gg \theta_0$: this situation (in which θ is much greater than both the boundary-dictated value and the flow-alignment angle) is not physically realisable if the liquid crystal is flow-aligning and no external torque is present.

Of the physically realistic cases, in two situations, namely Cases 1a and 2a, we will show that the equations simplify significantly and the solutions for u and θ are readily found to be quadratic and cubic polynomial functions of z , respectively. Case 2b is also tractable and we will show that in this case orientational boundary layers may exist.

The other two situations, namely Cases 1b and 1c, result in partial differential equations for θ that include derivatives in the x direction and fluid velocity in the z direction; these must, in general, be solved numerically. We will now consider shear-driven flow and pressure-driven flow separately.

III. SHEAR-DRIVEN FLOW

In this section we will consider shear-driven flow, that is, flow induced by moving the substrate parallel to itself with a constant velocity under a fixed blade of prescribed shape with no external pressure drop imposed.

A. Case 1a: $\epsilon \sim \delta \ll 1$ and $\delta \ll \theta_0$

In this case flow effects are insufficient to increase θ significantly from the boundary-dictated value and flow alignment is not achieved. Thus the orientational elasticity effects of the liquid crystal align the director. If we set $\delta = \epsilon$ then, in the limit $\epsilon \rightarrow 0$, Eqs. (16)–(18) become

$$0 = \tilde{p}_x - u_{zz} + O(\epsilon), \quad (28)$$

$$0 = \tilde{p}_z + O(\epsilon), \quad (29)$$

$$0 = E_\epsilon u_z + \theta_{zz} + O(\epsilon), \quad (30)$$

where we have introduced the appropriate Ericksen number $E_\epsilon = -\alpha_3 E/\epsilon$. (Note that the α_3 appearing here is non-dimensionalised with η_1 .) The boundary conditions are given by (22)–(25). Note that, since $\epsilon = \delta$, the leading order boundary condition on θ at $z = h$ is $\theta = h_x$.

From (30) we see that a well determined system is possible only if $E_\epsilon \ll 1$ or $E_\epsilon =$

$O(1)$. This is clear from the parameter ordering in this case: if we are to ensure that orientational elasticity effects dominate flow effects and that θ is therefore much less than the flow-alignment angle ($\delta \ll \theta_0$), then viscous terms should be dominated by elastic terms and therefore we cannot have $E_\epsilon \gg 1$. If $E_\epsilon \ll 1$ then the leading order term in (30) leads to a linear solution for θ and the flow has no effect on the director angle. In the remainder of this section we will concentrate on the more interesting case $E_\epsilon = O(1)$.

The velocity profile can be calculated directly from (28) and (29) to be

$$u = \frac{h-z}{h^3} [h^2 - 3(h-h_m)z], \quad (31)$$

where we have introduced the parameter $h_m = I_2/I_3$ with

$$I_n = \int_0^1 \frac{1}{h^n(x)} dx. \quad (32)$$

Note that the volume flux of fluid along the channel per unit width, Q , is given by $Q = h_m/2$.

Since θ does not enter (28) and (29) the leading order solution for the velocity given by (31) is exactly the same as that for a Newtonian fluid.³¹ From (31) we see that $u = 0$ not only at the blade $z = h$ but also on the curve $z = z_0$, where z_0 is given by

$$z_0 = \frac{h^2}{3(h-h_m)}, \quad (33)$$

and hence if $h > 3h_m/2$ there is a region of reverse flow (i.e. a region in which $u < 0$) between the curve $z = z_0$ and the blade $z = h$.

The sign of the shear may play an important role in the flow of a liquid crystal. When the shear is positive (negative) the flow will tend to align the director at the flow-alignment angle $+\theta_0$ ($-\theta_0$). From (31) we see that $u_z = 0$ on the curve $z = z_m$, where z_m is given by

$$z_m = \frac{h(4h-3h_m)}{6(h-h_m)}, \quad (34)$$

and hence if $h > 3h_m/2$ there is a region of reverse shear between the curve $z = z_m$ and the blade $z = h$ and if $h < 3h_m/4$ there is a region of reverse shear between the curve $z = z_m$ and the substrate $z = 0$.

Figure 3 shows the regions of the x - α parameter plane within which reverse flow and reverse shear occur for both the linearly converging channel $h(x) = 1 - \alpha(1 - x)$ with $\alpha < 0$ and the linearly diverging channel $h(x) = 1 + \alpha x$ with $\alpha > 0$. It is clear from Fig. 3 that there is a symmetry $(\alpha, x) \rightarrow (-\alpha, 1 - x)$; thus, the velocity profile for the linearly diverging channel can easily be constructed from that for the linearly converging channel. Note also that if the blade slope is sufficiently small in magnitude (specifically if $|\alpha| < 1$) then the regions of reverse flow and reverse shear do not occur.

Figure 4 shows the velocity profiles in the linearly converging and diverging channels with $\alpha = -2$ and $\alpha = 2$, respectively. In the case of the converging channel we have

$$h_m = \frac{2(\alpha - 1)}{\alpha - 2} = \frac{3}{2}, \quad (35)$$

and so when $h > 3h_m/2 = 9/4$, i.e. when

$$x < \frac{\alpha^2 - 1}{\alpha(\alpha - 2)} = \frac{3}{8}, \quad (36)$$

there is a region of reverse flow above the curve $z = z_0$ and a region of reverse shear above the curve $z = z_m$ (marked with a full line), and when $h < 3h_m/4 = 9/8$, i.e. when

$$x > \frac{(\alpha - 1)(2\alpha - 1)}{2\alpha(\alpha - 2)} = \frac{15}{16}, \quad (37)$$

there is a region of reverse shear below the curve $z = z_m$ (again marked with a full line).

In the case of the diverging channel we have

$$h_m = \frac{2(\alpha + 1)}{\alpha + 2} = \frac{3}{2}, \quad (38)$$

and so when $h > 3h_m/2 = 9/4$, i.e. when

$$x > \frac{2\alpha + 1}{\alpha(\alpha + 2)} = \frac{5}{8}, \quad (39)$$

there is a region of reverse flow above the curve $z = z_0$ and a region of reverse shear above the curve $z = z_m$ (marked with a full line), and when $h < 3h_m/4 = 9/8$, i.e. when

$$x < \frac{\alpha - 1}{2\alpha(\alpha + 2)} = \frac{1}{16}, \quad (40)$$

there is a region of reverse shear below the curve $z = z_m$ (again marked with a full line).

Substituting the solution (31) for u into the angular momentum balance (30), integrating twice and applying boundary conditions (22) and (23) leads to the solution for θ , namely

$$\theta = \frac{h_x}{h}z - E_\epsilon \frac{z(h-z)}{2h^3} [h(2h - h_m) - 2z(h - h_m)]. \quad (41)$$

Although orientational elasticity effects dominate flow effects and we expect the sign of the shear to have only a weak effect on the director angle, the solution (41) shows that flow changes the director angle from a linear to a cubic function of z .

The effect of flow on the director profile is shown in Figs. 5 and 6 in the linearly converging and diverging channels with $\alpha = -2$ and $\alpha = 2$, respectively. In the case of the converging channel with $\alpha < -1$, for values of E_ϵ lying in the range $0 < E_\epsilon < E_{\epsilon c1}$, where the critical value $E_{\epsilon c1}$ is given by

$$E_{\epsilon c1} = \frac{3\alpha^2(\alpha - 2)}{(\alpha - 1)(\alpha^2 - \alpha + 1)} = \frac{16}{7}, \quad (42)$$

the director profile is monotonic [Fig. 5(a)]. When E_ϵ is increased past this critical value the flow has a stronger effect and causes the director profile to develop a minimum and a maximum [Fig. 5(b)]. As E_ϵ increases further, past a second critical value $E_{\epsilon c2}$ given by

$$E_{\epsilon c2} = -\frac{\alpha(\alpha - 2)}{\alpha - 1} = \frac{8}{3}, \quad (43)$$

the maximum disappears and the director profile has only a minimum for all values of x [Fig. 5(c)]. The behaviour is slightly simpler when $-1 < \alpha < 0$. In this case there are no

reverse shear regions and the director profile changes from monotonic to non-monotonic at the critical Ericksen number E_{ec2} .

In the case of the diverging channel with $\alpha > 1$, for values of E_ϵ lying in the range $0 < E_\epsilon < E_{ec3}$, where the critical value E_{ec3} is given by

$$E_{ec3} = \frac{\alpha(\alpha + 2)}{(\alpha + 1)^2} = \frac{8}{9}, \quad (44)$$

the director profile is again monotonic [Fig. 6(a)]. When E_ϵ is increased past this critical value the flow has a stronger effect and causes the director profile to develop a minimum [Fig. 6(b)]. As E_ϵ increases further, past a second critical value E_{ec4} given by

$$E_{ec4} = \frac{2\alpha(\alpha + 2)}{\alpha + 1} = \frac{16}{3}, \quad (45)$$

the director profile also develops a maximum [Fig. 6(c)]. As E_ϵ increases further, past a third critical value E_{ec5} given by

$$E_{ec5} = \alpha(\alpha + 2) = 8, \quad (46)$$

the maximum disappears and the director profile has only a minimum for all values of x [Fig. 6(d)]. In a similar way to the previous case, the behaviour is slightly simpler when $0 < \alpha < 1$. In this case there are no reverse shear regions and the director profile changes from monotonic to non-monotonic at the critical Ericksen number E_{ec3} .

B. Case 2a: $\epsilon \ll \delta \ll 1$ and $\delta \ll \theta_0$

In this case flow effects increase θ significantly above the boundary-dictated value, but they are not sufficiently strong to achieve flow alignment. In the limit $\delta \rightarrow 0$, Eqs. (16)–(18) become

$$0 = \tilde{p}_x - u_{zz} + O(\delta), \quad (47)$$

$$0 = \tilde{p}_z + O(\delta), \quad (48)$$

$$0 = E_\delta u_z + \theta_{zz} + O(\delta), \quad (49)$$

where we have introduced the appropriate Ericksen number $E_\delta = -\alpha_3 E/\delta$. The boundary conditions are given by (22)–(25). Note that, since $\epsilon \ll \delta$, the leading order boundary condition on θ at $z = h$ is $\theta = 0$.

From (49) we see that a well determined system is possible only if $E_\delta \ll 1$ or $E_\delta = O(1)$. If $E_\delta \ll 1$ then the leading order term in (49) leads to the zero solution for θ and the flow has no effect on the director angle. In the remainder of this section we will concentrate on the more interesting case $E_\delta = O(1)$.

It follows from (28), (29), (47) and (48) that the leading order solution for the velocity is again given by (31). Thus the previous discussion of the regions of reverse flow and reverse shear again holds. Substituting the solution (31) for u into the angular momentum balance (49), integrating twice and applying boundary conditions (22) and (23) leads to the solution for θ , namely

$$\theta = -E_\delta \frac{z(h-z)}{2h^3} [h(2h-h_m) - 2z(h-h_m)]. \quad (50)$$

As in the previous section, although we expect the sign of the shear to have only a weak effect on the director angle, the solution (50) shows that flow changes the director angle from the zero solution to a cubic function of z .

The effect of the flow on the director profile is shown in Fig. 7 in the linearly converging and diverging channels with $\alpha = -2$ and $\alpha = 2$, respectively. From (50) we see that the Ericksen number E_δ enters the solution for the director angle only multiplicatively and that the director profile always has a minimum for all values of x . Although in Fig. 7 (and later in Figs. 10, 12 and 13) it appears that the director is not parallel to the blade at $z = h$, it should be borne in mind that we have plotted the blade using the scaled

function h^* ; if instead we had used the unscaled function $h = Hh^*$ (so that $h_x = \epsilon h_{x^*}^*$, with $\epsilon \ll \delta \ll 1$) then the blade slope would have been very small and it would have been clear that the leading-order boundary condition $\theta(x, h) = 0$ is appropriate.

C. Case 2b: $\epsilon \ll \delta \sim \theta_0 \ll 1$

In this case flow effects are sufficiently strong to achieve flow alignment in part of the channel. If we set $\delta = \theta_0$ then, in the limit $\theta_0 \rightarrow 0$, Eqs. (16)–(18) become

$$0 = \tilde{p}_x - u_{zz} + O(\theta_0), \quad (51)$$

$$0 = \tilde{p}_z + O(\theta_0), \quad (52)$$

$$0 = E_{\theta_0}(1 - \theta^2)u_z + \theta_{zz} + O(\theta_0), \quad (53)$$

where we have introduced the appropriate Ericksen number $E_{\theta_0} = -\alpha_3 E / \theta_0$. The boundary conditions are given by (22)–(25). Note that, since $\epsilon \ll \delta$, the leading order boundary condition on θ at $z = h$ is $\theta = 0$.

From (53) we see that if $E_{\theta_0} \ll 1$ then orientational elasticity effects dominate flow effects and at leading order θ is the zero solution. If $E_{\theta_0} = O(1)$ then orientational elasticity effects are comparable with flow effects and little analytical progress can be made because of the presence of the θ^2 term in (53). However, if $E_{\theta_0} \gg 1$ then flow effects dominate orientational elasticity effects, and $\theta = \pm 1$ (equivalent to the unscaled values $\pm\theta_0$) everywhere except in thin orientational boundary or internal layers over which θ changes rapidly. In the remainder of this section we will concentrate on the case $E_{\theta_0} \gg 1$.

The leading order solution for the velocity is again given by (31), and the regions of reverse flow and reverse shear found earlier are particularly important in this case in which flow effects align the director.

By substituting the solution (31) for u into the angular momentum balance (53), and performing a standard boundary-layer analysis³⁶ we determine the behaviour of θ near the boundaries. In the orientational boundary layer near $z = 0$ we introduce the boundary-layer variables Z and Θ defined by

$$Z = (|q_0|E_{\theta_0})^{1/2}z, \quad \Theta(Z) = -\text{sgn}(q_0)\theta(x, z), \quad (54)$$

where

$$q_0 = u_z|_{z=0} = \frac{3h_m - 4h}{h^2}. \quad (55)$$

Thus the orientational boundary layer near the substrate $z = 0$ is of thickness $O(E_{\theta_0}^{-1/2})$.

At leading order $\Theta(Z)$ satisfies

$$\Theta_{ZZ} = 1 - \Theta^2, \quad (56)$$

subject to $\Theta(0) = 0$ and $\Theta \rightarrow -1$ as $Z \rightarrow +\infty$, which can be solved analytically to give

$$\Theta = 2 - 3 \tanh^2 \left(\frac{Z}{\sqrt{2}} \pm \beta \right), \quad (57)$$

where $\beta = \tanh^{-1} \sqrt{2/3} \simeq 1.14622$. In Fig. 8 we plot Θ as a function of Z showing the structure of the boundary layer when we choose the plus sign in (57). Hence we find that the behaviour of the director inside the orientational boundary layer near $z = 0$ is given by

$$\theta \sim -\text{sgn}(q_0) \left[2 - 3 \tanh^2 \left(\left(\frac{|q_0|E_{\theta_0}}{2} \right)^{1/2} z \pm \beta \right) \right]. \quad (58)$$

In a similar way we find that the behaviour of the director inside the orientational boundary layer near $z = h$ is given by

$$\theta \sim -\text{sgn}(q_h) \left[2 - 3 \tanh^2 \left(\left(\frac{|q_h|E_{\theta_0}}{2} \right)^{1/2} (h - z) \pm \beta \right) \right], \quad (59)$$

where

$$q_h = u_z|_{z=h} = \frac{2h - 3h_m}{h^2}. \quad (60)$$

In particular, the orientational boundary layer near the blade $z = h$ is also of thickness $O(E_{\theta_0}^{-1/2})$.

Furthermore, if $h < 3h_m/4$ or $h > 3h_m/2$ then there exists a region of reverse shear in the channel (see Sec. III A) and the director profile develops an orientational internal layer within which the shear changes sign, and θ changes between its “outer” values of -1 and 1 . The orientational internal layer is near the curve $z = z_m$ given by (34) (i.e. the curve on which $u_z = 0$, indicated by the full lines in Fig. 4). We can analyse the behaviour of θ inside the orientational internal layer by introducing the inner variables ζ and ϕ defined by

$$\zeta = (|h - h_m|E_{\theta_0})^{1/3} \frac{z - z_m}{h}, \quad \phi(\zeta) = -\text{sgn}(h - h_m)\theta(x, z). \quad (61)$$

Thus the orientational internal layer near $z = z_m$ is of thickness $O(E_{\theta_0}^{-1/3})$. At leading order $\phi(\zeta)$ satisfies

$$\phi_{\zeta\zeta} = 6\zeta(1 - \phi^2), \quad (62)$$

subject to $\phi \rightarrow \pm 1$ as $\zeta \rightarrow \mp \infty$. This system for ϕ , which describes the behaviour of θ within the orientational internal layer, must be solved numerically; however, since it does not contain any parameters, it needs to be solved only once. We used a shooting method within the computer algebra package Maple to find an appropriate solution of this system. With $\phi(0) = 0$ we find that for $\phi_{\zeta}(0) > \phi_{\zeta c}$, where $\phi_{\zeta c} \simeq -1.51208$, the solutions are oscillatory, while for $\phi_{\zeta}(0) < \phi_{\zeta c}$ the solutions diverge to infinity. For “initial” conditions with $\phi(0) \neq 0$ other solutions are found; however, all of these solutions have higher energy than the solution with $\phi(0) = 0$ and $\phi_{\zeta}(0) = \phi_{\zeta c}$ and are therefore unlikely to be achieved in practice. Thus we will be concerned with only the numerically calculated solution of (62) with $\phi(0) = 0$ and $\phi_{\zeta}(0) = \phi_{\zeta c}$, which is shown in Fig. 9.

The regions of the x - α parameter plane within which an orientational internal layer

exists for both linearly converging ($\alpha < 0$) and linearly diverging ($\alpha > 0$) channels correspond to the regions of reverse shear shown in Fig. 3, since the orientational internal layer appears only when there is a change in the sign of the shear. In particular, Fig. 3 shows that there are no orientational internal layers when $|\alpha| < 1$. Furthermore, due to the symmetry $(\alpha, x) \rightarrow (-\alpha, 1 - x)$ the director profile for the linearly diverging channel can easily be constructed from that for the linearly converging channel.

A composite, uniformly valid leading order asymptotic solution for θ throughout the channel is found to be

$$\theta \sim - \left\{ \text{sgn}(q_0) \left[2 - 3 \tanh^2 \left(\left(\frac{|q_0| E_{\theta_0}}{2} \right)^{1/2} z \pm \beta \right) \right] + \text{sgn}(q_h) \left[2 - 3 \tanh^2 \left(\left(\frac{|q_h| E_{\theta_0}}{2} \right)^{1/2} (h - z) \pm \beta \right) \right] + \tilde{\phi}(\zeta) \right\}, \quad (63)$$

where

$$\tilde{\phi}(\zeta) = \begin{cases} -1 & \text{if } \frac{3}{4}h_m < h(x) < \frac{3}{2}h_m \\ \text{sgn}(h - h_m)\phi(\zeta) & \text{if } h(x) < \frac{3}{4}h_m \text{ or } h(x) > \frac{3}{2}h_m. \end{cases} \quad (64)$$

The choices of plus or minus signs in (63) lead to four distinct solutions. However, the choice of either of the minus signs corresponds to a solution with higher energy than the solution where both plus signs are chosen, and is therefore unlikely to be achieved in practice. We will therefore be concerned with only the solution (63) with both plus signs chosen.

Figure 10 shows the director profile in the linearly converging and diverging channels with $\alpha = -2$ and $\alpha = 2$, respectively, and clearly shows the orientational boundary and internal layer structures. In these particular linear channels $h_m = 3/2$ and the orientational internal layer exists when $h < 3h_m/4 = 9/8$ or $h > 3h_m/2 = 9/4$. Figure 10 also shows how the orientational internal layer merges with the upper boundary and reappears again from the lower boundary as x increases in the converging channel, or as

x decreases in the diverging channel. It is worth remarking that the asymptotic solution (63) was found to be in excellent agreement with the corresponding numerical solution of (53).

D. Case 1b: $\epsilon \sim \delta \sim \theta_0 \ll 1$ and Case 1c: $\theta_0 \ll \epsilon \sim \delta \ll 1$

In these cases orientational elasticity and flow effects are comparable. The leading order linear momentum balance is, in both cases, as in previous sections; thus the velocity is given again by (31). However, the angular momentum balance is given, in the two cases, by

$$0 = \theta_{zz} - E_{\theta_0} \left[-(1 - \theta^2) \theta_0^2 u_z + \epsilon \theta_0 (u \theta_x + w \theta_z + 2u_x \theta) - \epsilon^2 w_x \right] + O(\theta_0), \quad (65)$$

$$0 = \theta_{zz} - E_\epsilon (\theta^2 u_z + u \theta_x + w \theta_z + 2u_x \theta - w_x) + O(\epsilon), \quad (66)$$

respectively, where we have introduced the appropriate Ericksen numbers $E_{\theta_0} = -\alpha_2 E / \theta_0$ and $E_\epsilon = -\alpha_2 \epsilon E$. These nonlinear equations involve partial derivatives in both x and z and it seems that no analytical progress can be made. Some preliminary numerical results have been obtained by the authors using numerical methods designed to deal with boundary layers. However, this analysis is not pursued here.

IV. PRESSURE-DRIVEN FLOW

In this section we will consider pressure-driven flow, that is, flow induced by an imposed pressure drop across the fluid underneath a blade of prescribed shape with both the substrate and the blade fixed.

The governing equations are the same for shear-driven and pressure-driven flows, and hence we can proceed as before and obtain solutions for the velocity u that are

independent of the director angle θ . Specifically, the leading order solution for u subject to the appropriate boundary conditions (23) and (25)–(27) is found to be

$$u = \frac{z(h-z)}{2I_3h^3}, \quad (67)$$

where I_3 is again given by (32). From (67) we see that $u = 0$ only at the substrate $z = 0$ and at the blade $z = h$; thus, unlike in shear-driven flow, there are never any regions of reverse flow in the channel, that is, the fluid always flows in the direction of the imposed pressure drop. Also, from (67) we see that $u_z = 0$ on the curve $z = z_m = h/2$, and hence the shear always changes sign in the centre of the channel. Thus, there are always regions in the channel in which the shear is positive and regions in which is negative. The change in the sign of the shear will be important in the next three sections in which we will study the director orientation in response to pressure-driven flow in the different parameter regimes described in the shear-driven flow section.

Recalling that, in general, no analytical progress can be made in cases when orientational elasticity and flow effects are comparable (i.e. Cases 1b and 1c) we will again concentrate on the other three physically realistic cases.

A. Case 1a: $\epsilon \sim \delta \ll 1$ and $\delta \ll \theta_0$

In this case the governing equation for θ is given by (30) and the boundary conditions are given by (23) and (26). Note that the leading order boundary condition on θ at $z = h$ is $\theta = h_x$. The solution for θ can be calculated exactly to be

$$\theta = \frac{h_x}{h}z + E_\epsilon \frac{z(h-z)(h-2z)}{12I_3h^3}, \quad (68)$$

where $E_\epsilon = -\alpha_3 E/\epsilon$.

As in shear-driven flow, we see from the solution (68) that if $E_\epsilon \ll 1$ then θ is a linear function of z and if $E_\epsilon = O(1)$ then it is a cubic function of z . However, in this case

the effect of the flow on the director profile when $E_\epsilon = O(1)$ is slightly simpler than in shear-driven flow and there are only two possible profiles, both shown in Fig. 11 in the linearly converging and diverging channels with $\alpha = -2$ and $\alpha = 2$, respectively. In the case of the converging channel, for values of E_ϵ lying in the range $0 < E_\epsilon < E_{\epsilon c1}$, where the critical value $E_{\epsilon c1}$ is given by

$$E_{\epsilon c1} = \frac{6\alpha(\alpha - 2)}{(\alpha - 1)^2} = \frac{16}{3}, \quad (69)$$

the director profile is monotonic [Fig. 11(a)]. When E_ϵ is increased past this critical value the flow causes the director profile to develop a minimum and a maximum for all values of x [Fig. 11(b)]. In the case of the diverging channel, for values of E_ϵ lying in the range $0 < E_\epsilon < E_{\epsilon c2}$, where the critical value $E_{\epsilon c2}$ is given by

$$E_{\epsilon c2} = \frac{12\alpha(\alpha + 2)}{(\alpha + 1)^2} = \frac{32}{3}, \quad (70)$$

the director profile is again monotonic [Fig. 11(c)]. When E_ϵ is increased past this critical value the flow causes the director profile to develop a minimum and a maximum for all values of x [Fig. 11(d)].

B. Case 2a: $\epsilon \ll \delta \ll 1$ and $\delta \ll \theta_0$

In this case the governing equation for θ is given by (49), where again $E_\delta = -\alpha_3 E/\delta$, and the boundary conditions are given by (23) and (26). Note that the leading order boundary condition on θ at $z = h$ is $\theta = 0$. The solution for θ can again be calculated exactly to be

$$\theta = E_\delta \frac{z(h-z)(h-2z)}{12I_3 h^3}. \quad (71)$$

As in shear-driven flow, we see from the solution (71) that if $E_\delta \ll 1$ then θ is the zero solution and if $E_\delta = O(1)$ then it is a cubic function of z and E_δ enters the solution

for the director angle (71) only multiplicatively. However, whereas in shear-driven flow when $E_\delta = O(1)$ the director profile always has a minimum for all values of x , here it always has a minimum and a maximum.

Figure 12 shows the effect of the flow on the director profile in the linearly converging and diverging channels with $\alpha = -2$ and $\alpha = 2$, respectively.

C. Case 2b: $\epsilon \ll \delta \sim \theta_0 \ll 1$

In this case the governing equation for θ is given by (53), where again $E_{\theta_0} = -\alpha_3 E / \theta_0$, and the boundary conditions are given by (23) and (26). Note that the leading order boundary condition on θ at $z = h$ is $\theta = 0$.

As discussed in Sec. III C, we study the case $E_{\theta_0} \gg 1$, in which flow effects dominate orientational elasticity effects and $\theta = \pm 1$ everywhere except for thin orientational boundary or internal layers. We proceed as in Sec. III C performing a standard boundary-layer analysis and we find again that thin orientational boundary layers exist near the substrate and the blade, but that, unlike in shear-driven flow, a thin orientational internal layer always exists near the curve $z = z_m = h/2$ on which $u_z = 0$. Both boundary and internal layers have the same thickness as in shear-driven flow.

A composite, uniformly valid leading order asymptotic solution for θ throughout the channel is again given by (63) with

$$q_0 = u_z|_{z=0} = \frac{1}{2I_3 h^2} > 0, \quad q_h = u_z|_{z=h} = -\frac{1}{2I_3 h^2} < 0, \quad (72)$$

with ζ redefined by

$$\zeta = \left(\frac{E_{\theta_0}}{6I_3} \right)^{1/3} \frac{z - z_m}{h}, \quad (73)$$

and $\tilde{\phi} = -\phi$, where ϕ again satisfies (62) subject to the same boundary conditions.

Figure 13 shows the director profile in the linearly converging and diverging channels with $\alpha = -2$ and $\alpha = 2$, respectively, and, in particular, clearly shows the orientational boundary and internal layer structures.

V. DISCUSSION

We considered the steady, two-dimensional shear-driven and pressure-driven flow of a thin film of a nematic liquid crystal between a fixed blade of prescribed shape and a planar substrate. Simplified versions of the Ericksen–Leslie equations were obtained by assuming that both the aspect ratio of the slowly varying channel formed between the blade and the substrate and the distortion of the director field are small.

In the cases when orientational elasticity effects dominate flow effects (Cases 1a and 2a) we have found that the equations simplify significantly and the solutions for u and θ are quadratic and cubic polynomial functions of z , respectively. In these cases, critical values of the Ericksen number for which there is a qualitative change in the director profile are given explicitly. When orientational elasticity and flow effects are comparable (Cases 1b and 1c) the equations simplify to nonlinear partial differential equations that include derivatives in the x direction and fluid velocity in the z direction; these must, in general, be solved numerically. Finally, when flow effects dominate orientational elasticity effects (Case 2b) orientational boundary layers exist near the substrate and near the blade and, in addition, an orientational internal layer may also exist within the channel. In the case of shear-driven flow, if the blade slope remains below a critical value, $|\alpha| < 1$, the internal layer does not exist, whereas in the case of pressure-driven flow the internal layer always exists near the centre of the channel.

Velocity and director-orientation profiles have been shown for the particular choice

of a linear blade shape; however, it is possible to construct the velocity and director-orientation profiles for *any* nonlinear blade shape since the x coordinate enters (16)–(18) essentially as a parameter.

The detailed description of the director field given in this paper may help to improve coating and cell-filling techniques; in particular, it may indicate when defects are likely to occur in the final product.

We conclude with some final remarks concerning the Leslie viscosities α_2 and α_3 . Throughout this paper we assumed that $\alpha_2 < 0$ (as it is for calamitic liquid crystals) and $\alpha_3 < 0$, so that the material is flow-aligning, i.e. $\theta_0 = \tan^{-1} \sqrt{\alpha_3/\alpha_2}$ is defined. For flow-aligning nematic liquid crystals it is well known that the director can lie within the plane of shear, and thus the director field given by (1) is appropriate. On the other hand, if $\alpha_2 < 0$ and $\alpha_3 > 0$ then the liquid crystal is non-flow-aligning, i.e. θ_0 is not defined. In this case, the director may tend to leave the plane of shear. However, recent studies³⁷ have shown that a physically realisable solution for shear flow of a non-flow-aligning nematic liquid crystal with the director within the plane of shear is possible when the shear rate is low enough and the boundary conditions are appropriate. In such a case, the present analysis follows through with only minor differences. Finally, we note that although throughout the present work we restricted our attention to calamitic liquid crystals (for which $\alpha_2 < 0$), the present analysis is also relevant to *discotic* liquid crystals (i.e. liquid crystals whose constituent molecules are disc-like rather than rod-like) for which $\alpha_3 > 0$.³⁸ Specifically, the analysis for non-flow-aligning calamitics (with $\alpha_2 < 0$ and $\alpha_3 > 0$) also applies to non-flow-aligning discotics, and the analysis for flow-aligning calamitics (with $\alpha_2 < 0$ and $\alpha_3 < 0$) follows through to the case of flow-aligning discotics (with $\alpha_2 > 0$ and $\alpha_3 > 0$) with only minor differences.

ACKNOWLEDGEMENTS

NJM wishes to thank EPSRC for financial support via an Advanced Research Fellowship, and JQC wishes to thank the University of Strathclyde for financial support via a Graduate Teaching Assistantship.

APPENDIX: DERIVATION OF THE THIN-FILM APPROXIMATION

In this appendix we give a derivation of the thin-film equations (16)–(18). For a steady two-dimensional solution of the form (1)–(3), with inertia and external forces neglected, it is found that the constitutive laws for W , $\tilde{\mathbf{g}}$ and $\tilde{\mathbf{t}}$ reduce to

$$2W = K_1(-\sin\theta\theta_x + \cos\theta\theta_z)^2 + K_3(\cos\theta\theta_x + \sin\theta\theta_z)^2, \quad (\text{A.1})$$

$$\tilde{\mathbf{g}} = -\gamma_1 N(-\mathbf{i}\sin\theta + \mathbf{k}\cos\theta) - \gamma_2 \left[u_x(\mathbf{i}\cos\theta - \mathbf{k}\sin\theta) + \frac{1}{2}(u_z + w_x)(\mathbf{i}\sin\theta + \mathbf{k}\cos\theta) \right], \quad (\text{A.2})$$

and

$$\tilde{t}_{i2} = \tilde{t}_{2i} = 0, \quad (\text{A.3})$$

$$\begin{aligned} \tilde{t}_{11} = & \alpha_1 A \cos^2\theta - (\alpha_2 + \alpha_3)N \sin\theta \cos\theta \\ & + \alpha_4 u_x + (\alpha_5 + \alpha_6) \left[u_x \cos^2\theta + \frac{1}{2}(u_z + w_x) \sin\theta \cos\theta \right], \end{aligned} \quad (\text{A.4})$$

$$\begin{aligned} \tilde{t}_{13} = & \alpha_1 A \cos\theta \sin\theta + (\alpha_3 \cos^2\theta - \alpha_2 \sin^2\theta)N \\ & + \frac{1}{2}(\alpha_4 + \alpha_5 \sin^2\theta + \alpha_6 \cos^2\theta)(u_z + w_x) + (\alpha_5 - \alpha_6)u_x \cos\theta \sin\theta, \end{aligned} \quad (\text{A.5})$$

$$\begin{aligned} \tilde{t}_{31} = & \alpha_1 A \cos\theta \sin\theta + (\alpha_2 \cos^2\theta - \alpha_3 \sin^2\theta)N \\ & + \frac{1}{2}(\alpha_4 + \alpha_5 \cos^2\theta + \alpha_6 \sin^2\theta)(u_z + w_x) - (\alpha_5 - \alpha_6)u_x \cos\theta \sin\theta, \end{aligned} \quad (\text{A.6})$$

$$\begin{aligned} \tilde{t}_{33} = & \alpha_1 A \sin^2\theta + (\alpha_2 + \alpha_3)N \sin\theta \cos\theta \\ & - \alpha_4 u_x - (\alpha_5 + \alpha_6) \left[u_x \sin^2\theta - \frac{1}{2}(u_z + w_x) \sin\theta \cos\theta \right], \end{aligned} \quad (\text{A.7})$$

where we have introduced

$$N = u\theta_x + w\theta_z + \frac{1}{2}(u_z - w_x), \quad (\text{A.8})$$

$$A = (\cos^2 \theta - \sin^2 \theta)u_x + \sin \theta \cos \theta(u_z + w_x). \quad (\text{A.9})$$

Hence the linear momentum and the angular momentum balances in the Ericksen–Leslie equations (5) and (6) give

$$0 = -\tilde{p}_x + \Gamma\theta_x + \tilde{t}_{11,x} + \tilde{t}_{13,z}, \quad (\text{A.10})$$

$$0 = -\tilde{p}_z + \Gamma\theta_z + \tilde{t}_{31,x} + \tilde{t}_{33,z}, \quad (\text{A.11})$$

$$\left(\frac{\partial W}{\partial \theta_x}\right)_x + \left(\frac{\partial W}{\partial \theta_z}\right)_z - \frac{\partial W}{\partial \theta} + \Gamma = 0, \quad (\text{A.12})$$

where we have introduced

$$\Gamma = -\gamma_1 N - \gamma_2 \left[-2u_x \sin \theta \cos \theta + \frac{1}{2}(u_z + w_x)(\cos^2 \theta - \sin^2 \theta)\right]. \quad (\text{A.13})$$

Furthermore, the angular momentum balance (A.12) can be written as

$$\begin{aligned} & (K_1 \sin^2 \theta + K_3 \cos^2 \theta)\theta_{xx} + (K_1 \cos^2 \theta + K_3 \sin^2 \theta)\theta_{zz} \\ & + (K_3 - K_1)[(\cos \theta \theta_x + \sin \theta \theta_z)(-\sin \theta \theta_x + \cos \theta \theta_z) + 2 \sin \theta \cos \theta \theta_{xz}] + \Gamma = 0. \end{aligned} \quad (\text{A.14})$$

We denote the “scale” of any quantity by means of square brackets, and recalling the non-dimensionalisation in (12) and (13) for shear-driven flow we have

$$[\tilde{p}_x] = \frac{\mu_0 U}{H^2}, \quad [\tilde{p}_z] = \frac{\mu_0 U L}{H^3}. \quad (\text{A.15})$$

We now consider the case when $\epsilon = H/L \ll 1$; in this case the following scales are found:

$$[N] = \frac{U}{H}, \quad [A] = \frac{U}{H}, \quad (\text{A.16})$$

$$[\Gamma] = \frac{\mu_0 U}{H}, \quad [\Gamma\theta_x] = \frac{\mu_0 U}{HL}, \quad [\Gamma\theta_z] = \frac{\mu_0 U}{H^2}, \quad (\text{A.17})$$

$$[\tilde{t}_{ij}] = \frac{\mu_0 U}{H}, \quad [\tilde{t}_{ij,x}] = \frac{\mu_0 U}{HL}, \quad [\tilde{t}_{ij,z}] = \frac{\mu_0 U}{H^2}, \quad (i, j = 1, 3), \quad (\text{A.18})$$

$$[W] = \frac{K_0}{H^2}. \quad (\text{A.19})$$

(In fact, from (12) and (14) the corresponding scales for pressure-driven flow are also given by (A.15)–(A.19), with U replaced by $H^2(p_0 - p_L)/\mu_0 L$.) This enables us to make the following approximations:

$$N \sim \frac{1}{2}u_z, \quad (\text{A.20})$$

$$A \sim \cos \theta \sin \theta u_z, \quad (\text{A.21})$$

$$\Gamma \sim -m(\theta)u_z, \quad (\text{A.22})$$

with $m(\theta)$ given by (21),

$$\tilde{t}_{13} \sim g(\theta)u_z, \quad (\text{A.23})$$

with $g(\theta)$ given by (19), and

$$W \sim \frac{1}{2}f(\theta)\theta_z^2, \quad (\text{A.24})$$

with $f(\theta)$ given by (20). Hence, it follows that at leading order in ϵ equations (A.10)–(A.12) simplify to the thin-film equations (16)–(18) introduced in Sec. II A.

¹ R. Penterman, S. I. Klink, H. de Koning, G. Nisato and D. J. Broer, “Single-substrate liquid-crystal displays by photo-enforced stratification,” *Nature* **417**, 55 (2002).

² J. L. Ericksen, “Anisotropic fluids,” *Arch. Ration. Mech. Anal.* **4**, 231 (1960).

³ F. M. Leslie, “Some constitutive equations for anisotropic fluids,” *Q. J. Mech. Appl. Math.* **19**, 357 (1966).

⁴ P. G. de Gennes and J. Prost, *The Physics of Liquid Crystals*, 2nd ed. (Oxford University Press, London, 1993).

- ⁵ I. W. Stewart, *The Static and Dynamic Continuum Theory of Liquid Crystals* (Taylor and Francis, London and New York, 2004).
- ⁶ S. A. Pikin, “Couette flow of a nematic liquid,” *Sov. Phys. JETP* **38**, 1246 (1974).
- ⁷ G. P. MacSithigh and P. K. Currie, “Apparent viscosity during simple shearing flow of nematic liquid crystals,” *J. Phys. D* **10**, 1471 (1977).
- ⁸ P. K. Currie and G. P. MacSithigh, “The stability and dissipation of solutions for shearing flow of nematic liquid crystals,” *Q. J. Mech. Appl. Math.* **32**, 499 (1979).
- ⁹ K. Skarp and T. Carlsson, “Influence of an electric field on the flow alignment angle in shear flow of nematic liquid crystals,” *Mol. Cryst. Liq. Cryst.* **49**, 75 (1978).
- ¹⁰ R. J. Atkin, “Poiseuille flow of liquid crystals of the nematic type,” *Arch. Ration. Mech. Anal.* **38**, 224 (1970).
- ¹¹ P. K. Currie, “Approximate solutions for Poiseuille flow of liquid crystals,” *Rheol. Acta* **14**, 688 (1975).
- ¹² A. D. Rey and M. M. Denn, “Jeffrey–Hamel flow of Leslie–Ericksen nematic liquids,” *J. Non-Newtonian Fluid Mech.* **27**, 375 (1988).
- ¹³ G. Derfel, “Development of the shear flow induced deformation in nematic layers,” *Mol. Cryst. Liq. Cryst.* **191**, 377 (1990).
- ¹⁴ G. Derfel and B. Radomska, “Modelling of the simple shear flow of a flow-aligning nematic,” *Liq. Cryst.* **23**, 741 (1997).
- ¹⁵ H. Tu, G. Goldbeck-Wood and A. H. Windle, “Simulation of texture evolution for nematic liquid crystalline polymers under shear flow,” *Liq. Cryst.* **29**, 335 (2002).
- ¹⁶ A. D. Rey, “Orientational transition in radial flow of a nematic liquid,” *J. Non-Newtonian Fluid Mech.* **40**, 177 (1991).
- ¹⁷ S. Chono and T. Tsuji, “Numerical simulation of nematic liquid crystalline flows around a

- circular cylinder,” *Mol. Cryst. Liq. Cryst.* **309**, 217 (1998).
- ¹⁸ R.-Y. Chang, F.-C. Shiao and W.-L. Yang, “Simulation of director orientation of liquid crystalline polymers in 2-D flows,” *J. Non-Newtonian Fluid Mech.* **55**, 1 (1994).
- ¹⁹ W. R. Burghardt and G. G. Fuller, “Transient shear flow of nematic liquid crystals: manifestations of director tumbling,” *J. Rheol.* **34**, 959 (1990).
- ²⁰ W. H. Han and A. D. Rey, “Supercritical bifurcations in simple shear flow of a non-aligning nematic: reactive parameter and director anchoring effects,” *J. Non-Newtonian Fluid Mech.* **48**, 181 (1993).
- ²¹ J. Tao and J. J. Feng, “Effects of elastic anisotropy on the flow and orientation of sheared nematic liquid crystals,” *J. Rheol.* **47**, 1051 (2003).
- ²² A. P. Krekhov, L. Kramer, A. Buka and A. N. Chuvirov, “Flow alignment of nematics under oscillatory shear,” *J. Phys. II* **3**, 1387 (1993).
- ²³ L. R. P. de Andrade Lima and A. D. Rey, “Assessing flow alignment of nematic liquid crystals through linear viscoelasticity,” *Phys. Rev. E* **70**, 011701 (2004).
- ²⁴ J. L. Ericksen, “Liquid crystals with variable degree of orientation,” *Arch. Ration. Mech. Anal.* **113**, 97 (1991).
- ²⁵ M. C. Calderer and C. Liu, “Poiseuille flow of nematic liquid crystals,” *Int. J. Eng. Sci.* **38**, 1007 (2000).
- ²⁶ J. Feng and L. G. Leal, “Pressure-driven channel flows of a model liquid-crystalline polymer,” *Phys. Fluids* **11**, 2821 (1999).
- ²⁷ A. D. Rey and T. Tsuji, “Recent advances in theoretical liquid crystal rheology,” *Macromol. Theory Simul.* **7**, 623 (1998).
- ²⁸ A. D. Rey and M. M. Denn, “Dynamical phenomena in liquid-crystalline materials,” *Annu. Rev. Fluid Mech.* **34**, 233 (2002).

- ²⁹ J. Quintans Carou, B. R. Duffy, N. J. Mottram and S. K. Wilson, “Steady flow of a nematic liquid crystal in a slowly varying channel,” *Mol. Cryst. Liq. Cryst.* (Proceedings of the 20th International Liquid Crystal Conference, Ljubljana, Slovenia, 4–9 July 2004) (to appear).
- ³⁰ D. A. Dunmur, A. Fukuda and G. Luckhurst, *Physical Properties of Liquid Crystals: Nematics* (INSPEC, London, 2000).
- ³¹ H. Ockendon and J. R. Ockendon, *Viscous Flow* (Cambridge University Press, Cambridge, 1995).
- ³² M. Ben Amar and L. J. Cummings, “Fingering instabilities in driven thin nematic films,” *Phys. Fluids* **13**, 1160 (2001).
- ³³ M. Miesowicz, “The three coefficients of viscosity of anisotropic liquids,” *Nature* **17**, 261 (1935).
- ³⁴ A. D. Rey, “The Neumann and Young equations for nematic contact lines,” *Liq. Cryst.* **27**, 195 (2000).
- ³⁵ A. Poniewierski, “Shape of the nematic-isotropic interface in conditions of partial wetting,” *Liq. Cryst.* **27**, 1369 (2000).
- ³⁶ A. H. Nayfeh, *Perturbation Methods* (Wiley, New York, 1973).
- ³⁷ T. Carlsson and C. Högfors, “Theoretical analysis of the stability of shear flow of nematic liquid crystals with a positive Leslie viscosity α_3 ,” *J. Non-Newtonian Fluid Mech.* **119**, 25 (2004).
- ³⁸ S. Chandrasekhar, “Columnar, discotic nematic and lamellar liquid crystals: their structures and physical properties” Chapter 8 in “*Handbook of Liquid Crystals, Vol. 2B, Low Molecular Weight Liquid Crystals II*”, edited by D. Demus, J. Goodby, G. W. Gray, H.-W. Spiess and V. Vill (Wiley-VCH, Weinheim, 1998).

LIST OF FIGURE CAPTIONS

Figure 1: Geometry of the blade-coating process. The substrate is moved to the right in order to coat it with a thin film of liquid crystal.

Figure 2: Geometry of the mathematical model of a nematic liquid crystal in a slowly varying channel under a fixed blade.

Figure 3: The x - α parameter plane showing the regions within which reverse flow and reverse shear occur in shear-driven flow for both linearly converging ($\alpha < 0$) and linearly diverging ($\alpha > 0$) channels.

Figure 4: Velocity profiles in shear-driven flow in the cases (a) $h(x) = 1 - \alpha(1 - x)$ with $\alpha = -2$, and (b) $h(x) = 1 + \alpha x$ with $\alpha = 2$, at $x = 0, 0.2, 0.4, 0.6, 0.8, 1$. Reverse shear occurs above the curve $z = z_m$ on which $u_z = 0$ (indicated by full lines) when $h > 9/4$ and below $z = z_m$ when $h < 9/8$.

Figure 5: The director angle θ in shear-driven flow in Case 1a when $h(x) = 1 - \alpha(1 - x)$ with $\alpha = -2$, and (a) $E_\epsilon = 1$, (b) $E_\epsilon = 2.5$ and (c) $E_\epsilon = 3$. The curve on which $\theta_z = 0$ is indicated by a full line (for a local minimum) and a dotted line (for a local maximum).

Figure 6: The director angle θ in shear-driven flow in Case 1a when $h(x) = 1 + \alpha x$ with $\alpha = 2$, and (a) $E_\epsilon = 0.5$, (b) $E_\epsilon = 3$, (c) $E_\epsilon = 6.5$ and (d) $E_\epsilon = 9$. The curve on which $\theta_z = 0$ is indicated by a full line (for a local minimum) and a dotted line (for a local maximum).

Figure 7: The director angle θ in shear-driven flow in Case 2a when (a) $h(x) = 1 - \alpha(1 - x)$ with $\alpha = -2$, and (b) $h(x) = 1 + \alpha x$ with $\alpha = 2$, and $E_\delta = 2.5$. The curve on which $\theta_z = 0$ is indicated by a full line. Scaled variables are plotted, and so the leading-order boundary condition $\theta(x, h) = 0$ is appropriate, even though it appears that the director is not parallel to the blade at $z = h$.

Figure 8: Plot of Θ as a function of Z given by (57) with the plus sign, showing the structure of the orientational boundary layer in Case 2b.

Figure 9: Plot of ϕ as a function of ζ given by the numerical solution of (62) with $\phi(0) = 0$ and $\phi_\zeta(0) = \phi_{\zeta c} \simeq -1.51208$, showing the structure of the orientational internal layer in Case 2b.

Figure 10: The director angle θ in shear-driven flow in Case 2b when (a) $h(x) = 1 - \alpha(1 - x)$ with $\alpha = -2$, and (b) $h(x) = 1 + \alpha x$ with $\alpha = 2$, and $E_{\theta_0} = 10^4$. The curve $z = z_m$ on which $u_z = 0$ is indicated by a full line. Scaled variables are plotted, and so the leading-order boundary condition $\theta(x, h) = 0$ is appropriate, even though it appears that the director is not parallel to the blade at $z = h$.

Figure 11: The director angle θ in pressure-driven flow in Case 1a when $h(x) = 1 - \alpha(1 - x)$ with $\alpha = -2$, and $h(x) = 1 + \alpha x$ with $\alpha = 2$, and (a) $E_\epsilon = 3$ and (b) $E_\epsilon = 15$ in the case of a converging channel and (c) $E_\epsilon = 5$ and (d) $E_\epsilon = 15$ in the case of a diverging channel. The curve on which $\theta_z = 0$ is indicated by a full line (for a local minimum) and a dotted line (for a local maximum).

Figure 12: The director angle θ in pressure-driven flow in Case 2a when (a) $h(x) = 1 - \alpha(1 - x)$ with $\alpha = -2$, and (b) $h(x) = 1 + \alpha x$ with $\alpha = 2$, and $E_\delta = 6$. The curve on which $\theta_z = 0$ is indicated by a full line (for a local minimum) and a dotted line (for a local maximum). Scaled variables are plotted, and so the leading-order boundary condition $\theta(x, h) = 0$ is appropriate, even though it appears that the director is not parallel to the blade at $z = h$.

Figure 13: The director angle θ in pressure-driven flow in Case 2b when (a) $h(x) = 1 - \alpha(1 - x)$ with $\alpha = -2$, and (b) $h(x) = 1 + \alpha x$ with $\alpha = 2$, and $E_{\theta_0} = 10^4$. The curve $z = z_m = h/2$ on which $u_z = 0$ is indicated by a full line. Scaled variables are plotted, and so the leading-order boundary condition $\theta(x, h) = 0$ is appropriate, even though it

appears that the director is not parallel to the blade at $z = h$.

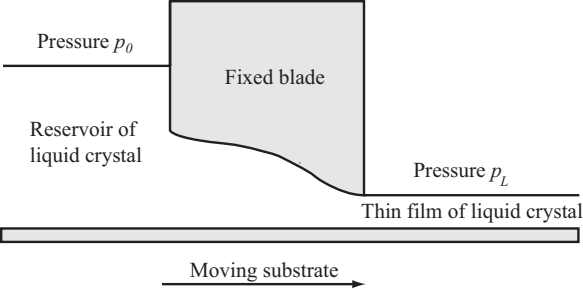


Figure 1, Quintans Carou, *Phys. Fluids*

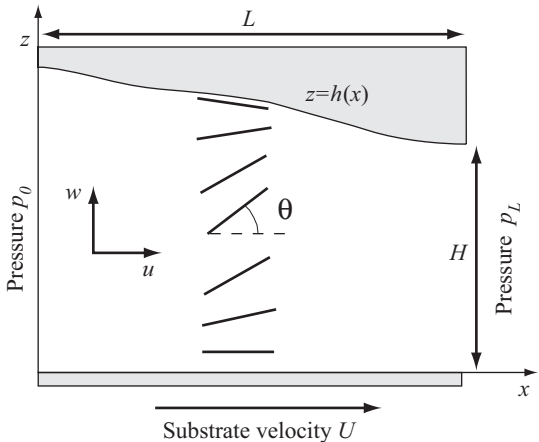


Figure 2, Quintans Carou, *Phys. Fluids*

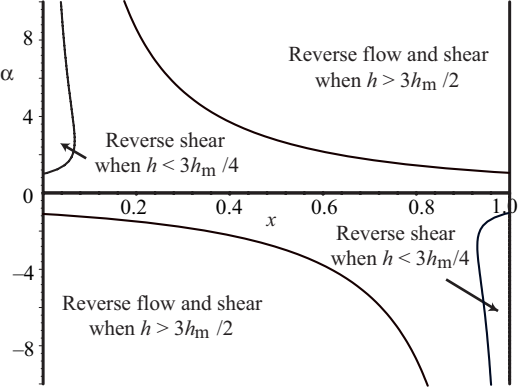


Figure 3, Quintans Carou, *Phys. Fluids*

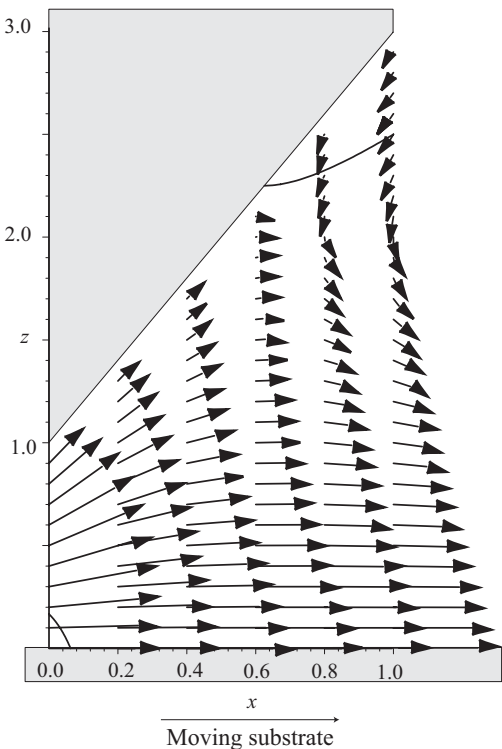
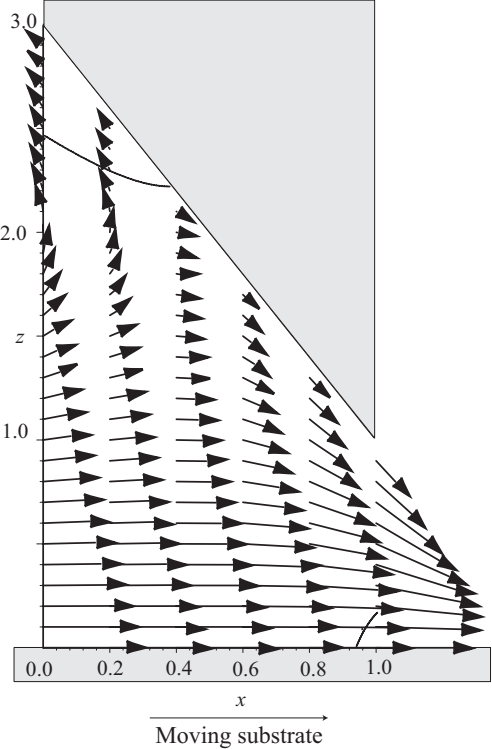
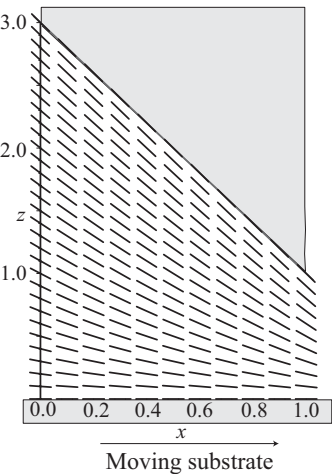
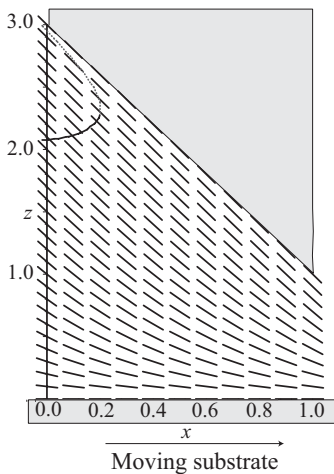


Figure 4, Quintans Carou, *Phys. Fluids*

(a) $E_\varepsilon = 1$



(b) $E_\varepsilon = 2.5$



(c) $E_\varepsilon = 3$

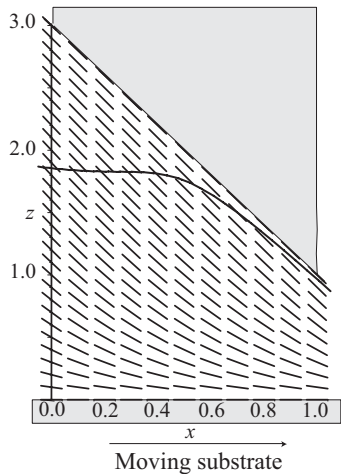
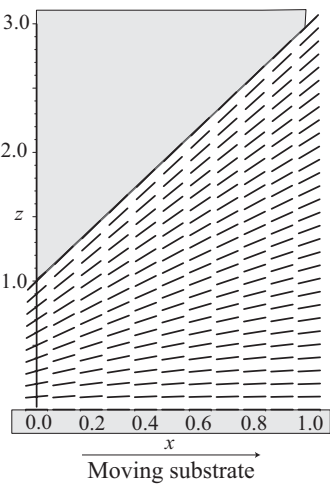
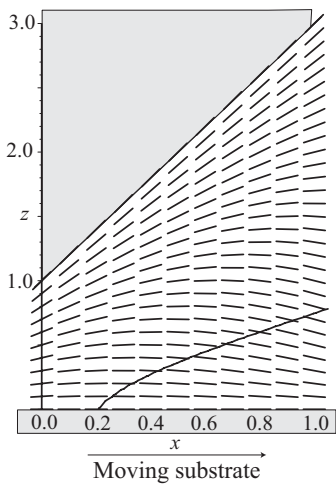


Figure 5, Quintans Carou, *Phys. Fluids*

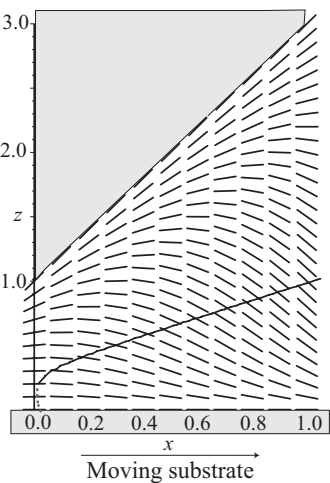
(a) $E_\varepsilon = 0.5$



(b) $E_\varepsilon = 3$



(c) $E_\varepsilon = 6.5$



(d) $E_\varepsilon = 9$

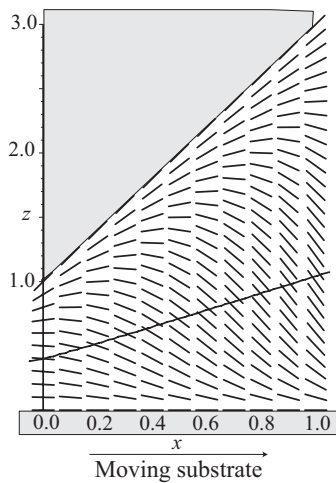


Figure 6, Quintans Carou, *Phys. Fluids*

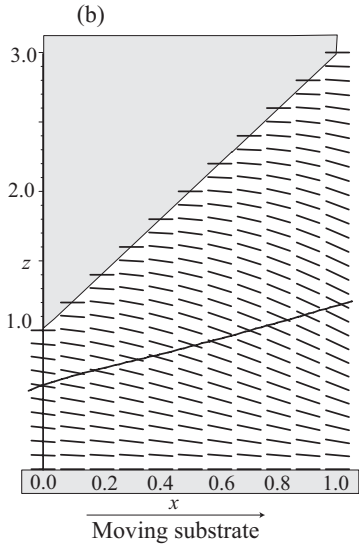
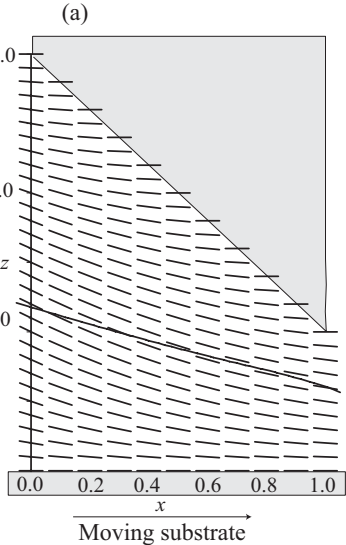


Figure 7, Quintans Carou, *Phys. Fluids*

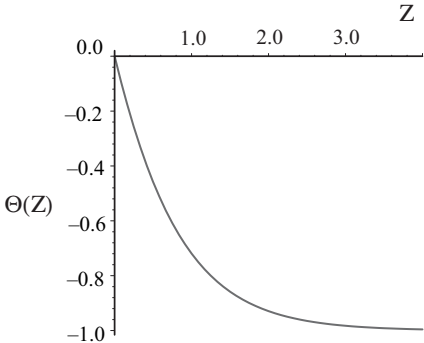


Figure 8, Quintans Carou, *Phys. Fluids*

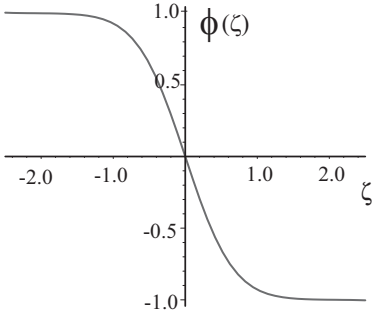


Figure 9, Quintans Carou, *Phys. Fluids*

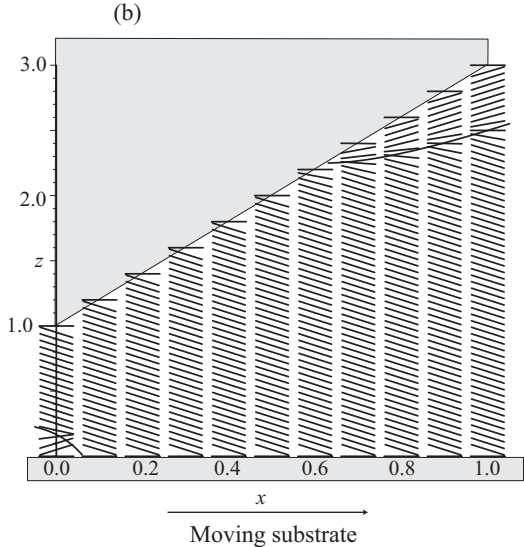
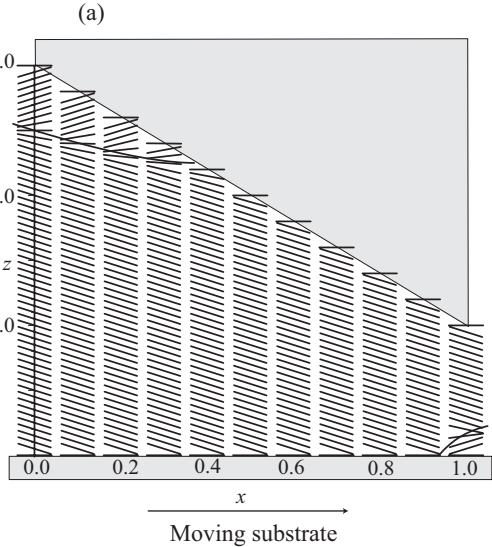
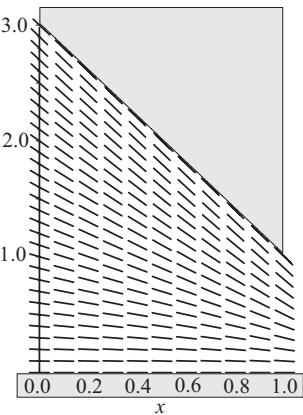
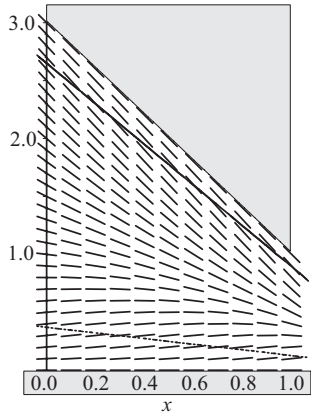


Figure 10, Quintans Carou, *Phys. Fluids*

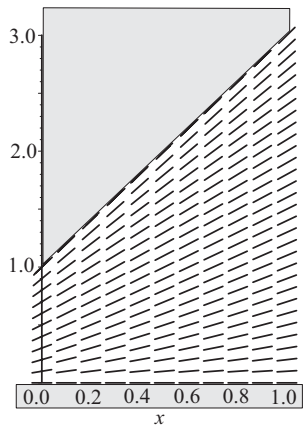
(a) $E_\varepsilon = 3$



(b) $E_\varepsilon = 15$



(c) $E_\varepsilon = 5$



(d) $E_\varepsilon = 15$

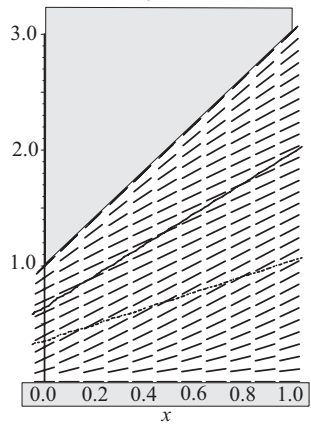
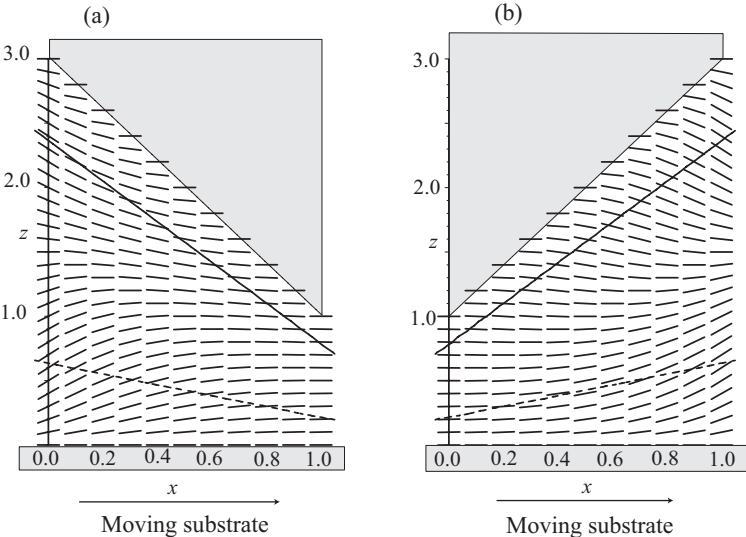


Figure 11, Quintans Carou, *Phys. Fluids*



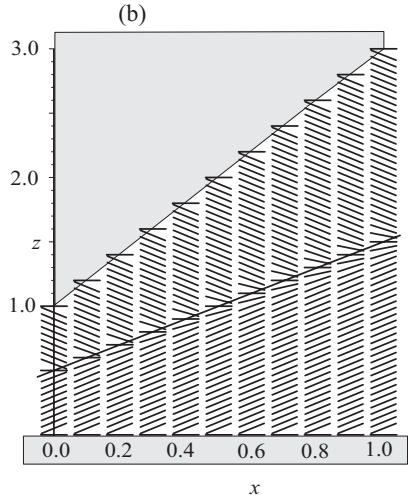
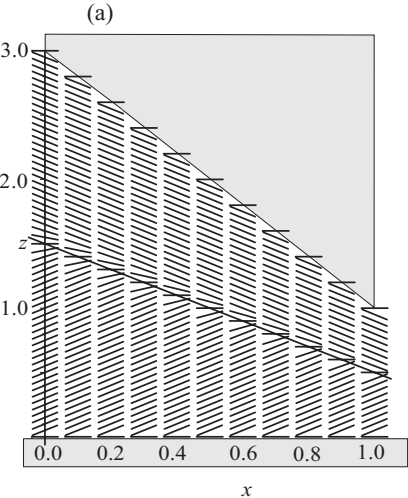


Figure 13, Quintans Carou, *Phys. Fluids*